2021

Inhibitor of growth protein 3 epigenetically silences endogenous retroviral elements and prevents innate immune activation

Yanhua Song

Gaopeng Hou

Jonathan Diep

Yaw Shin Ooi

Natalia S. Akopyants

See next page for additional authors

Authors

Yanhua Song, Gaopeng Hou, Jonathan Diep, Yaw Shin Ooi, Natalia S. Akopyants, Stephen M. Beverley, Jan E. Carette, Harry B. Greenberg, and Siyuan Ding

12706–12715 *Nucleic Acids Research, 2021, Vol. 49, No. 22* *Published online 17 November 2021*
https://doi.org/10.1093/nar/gkab1070

Inhibitor of growth protein 3 epigenetically silences endogenous retroviral elements and prevents innate immune activation

Yanhua Song[1,2,3,4,†], Gaopeng Hou[5,†], Jonathan Diep[1], Yaw Shin Ooi[1], Natalia S. Akopyants[5], Stephen M. Beverley[5], Jan E. Carette[1], Harry B. Greenberg[1,2,3] and Siyuan Ding[5,*]

[1]Department of Microbiology and Immunology, Stanford University, Stanford, CA, USA, [2]Department of Medicine, Division of Gastroenterology and Hepatology, Stanford University, Stanford, CA, USA, [3]Palo Alto Veterans Institute of Research, VA Palo Alto Health Care System, Palo Alto, CA, USA, [4]Institute of Veterinary Medicine, Jiangsu Academy of Agricultural Sciences, Nanjing, China and [5]Department of Molecular Microbiology, Washington University School of Medicine in St. Louis, St. Louis, MO, USA

Received January 26, 2021; Revised October 13, 2021; Editorial Decision October 15, 2021; Accepted October 19, 2021

ABSTRACT

Endogenous retroviruses (ERVs) are subject to transcriptional repression in adult tissues, in part to prevent autoimmune responses. However, little is known about the epigenetic silencing of ERV expression. Here, we describe a new role for inhibitor of growth family member 3 (ING3), to add to an emerging group of ERV transcriptional regulators. Our results show that ING3 binds to several ERV promoters (for instance *MER21C*) and establishes an EZH2-mediated H3K27 trimethylation modification. Loss of ING3 leads to decreases of H3K27 trimethylation enrichment at ERVs, induction of MDA5-MAVS-interferon signaling, and functional inhibition of several virus infections. These data demonstrate an important new function of ING3 in ERV silencing and contributing to innate immune regulation in somatic cells.

INTRODUCTION

Transposable elements (TEs) consist of repetitive nucleic acid sequences that make up as much as 40–60% of the mammalian genome (1,2). TEs are composed of DNA transposons and retrotransposons, which can be further categorized into elements with long terminal repeats (LTRs) such as endogenous retroviruses (ERVs) and TEs without LTRs such as long interspersed nuclear elements (LINEs) or short interspersed nuclear elements (SINEs) (3).

ERVs share substantial similarities with exogenous retroviral proviruses and are implicated in embryonic development, autoimmune diseases, and neurological disorders (4–6). Therefore, ERV transcription needs to be tightly regulated to provide genomic stability and avoid aberrant expression of neighboring genes and oncogenic transformation (7). However, only a handful of ERV regulators are known, including zinc-finger protein Zfp809, Trim28, Setdb1, Snerv and the HUSH complex, which epigenetically silence mouse ERV activation via H3K9 trimethylation (8–14). Even fewer epigenetic silencers are known for human ERVs: TRIM28 (11), TIP60 (14) and more recently KDM5B (15) and FBXO44 (16). Low expression of KDM5B or FBXO44 has been associated with ERV reactivation and an accelerated immune clearance of tumors (15,16). The suppressive mechanisms of most human ERVs in the genome remain largely unknown.

Inhibitor of Growth Family Member 3 (encoded by ING3) is a member of the ING tumor suppressor family (17) and encodes a plant homeodomain (PHD) finger, a motif common to chromatin-regulatory proteins. ING3 is found to be recruited to double-strand DNA breaks and contributes to DNA repair (18). ING3 is a key subunit of the human NuA4/Tip60 histone acetyltransferases complex (17). Recently, it was shown that TIP60 represses activation of ERV elements, which turns on STING-IRF7 mediated inflammatory responses (14). This suggested to us that ING3 may also participate in regulating ERV expression. However, there is little, if any, information on how ING3 may potentially impact virus infection and host innate immunity. In the current study, through a series of genetic, biochemical and functional experiments, we found

*To whom correspondence should be addressed. Tel: +1 314 273 3963; Fax: +1 314 362 1232; Email: siyuan.ding@wustl.edu
†The authors wish it to be known that, in their opinion, the first two authors should be regarded as Joint First Authors.
Present address: Yaw Shin Ooi, Program in Emerging Infectious Diseases, Duke-National University of Singapore Medical School, Singapore, Singapore.

that in cells lacking ING3, multiple ERV expression was re-activated and MDA5-MAVS signaling pathway was induced, which altogether identified ING3 to be a novel transcriptional repressor of ERVs.

MATERIALS AND METHODS

Cells, plasmids, and reagents

H1-Hela cells (CRL-1958) were obtained from American Type Culture Collection (ATCC) and cultured in complete Dulbecco's modified Eagle's medium (DMEM) medium. HT-29 cells (HTB38) were obtained from ATCC and cultured in complete advanced DMEM/F12 medium. *ING3* KO HT-29 cells were transduced with pLenti-C-Myc-DDK-P2A-Puro empty vector, pLenti-C-Myc-DDK-P2A-ING3, pLenti-C-mGFP empty vector, or pLenti-C-mGFP-ING3 and cultured under puromycin selection (1 μg/ml). pSpCas9(BB)-2A-GFP (PX458) and lenti-CRISPR_v2 were purchased from Addgene (48138 and 52961, respectively). Ruxolitinib (Selleckchem, S1378) was reconstituted at 10 mM stock solution in dimethyl sulfoxide (DMSO) and used at 100 nM in cell culture. Recombinant human IFN-β was purchased from R&D Systems (285-IF-100). Poly(I:C) high molecular weight (InvivoGen, tlrl-piclv), LyoVec (InvivoGen, lyec-12), GSK126 (Selleckchem, S7061), JIB-04 (Tocris, 4972), and GSK-J4 (Tocris, 4594) were purchased from respective vendors.

CRISPR/Cas9 knockout cells

Single clonal knockout HT-29 cells were obtained using the PX458 vector that expresses Cas9 and single-guide RNA (sgRNA) against *ING3* (Supplementary Table S1). Green fluorescent protein (GFP)-positive single cells were sorted at 48 h post-transfection using BD Aria II into 96-well plates and screened for knockout based on western blot and Sanger sequencing using primers listed in Supplementary Table S1. Pooled knockout H1-Hela cells were obtained by lentiviral transduction with the lenti-CRISPR_v2 vector that expresses Cas9 and sgRNA against *CHD8*, *COG7*, *ING3*, *KDSR*, *MGAT1*, *MMGT1*, *MYC*, *PHIP*, or *RALGAPB* for 14 days under puromycin selection (10 μg/ml). Pooled knockout HT-29 cells were obtained by lentiviral transduction of *ING3* KO HT-29 cells with the lenti-CRISPR_v2 vector that expresses Cas9 and sgRNA against RIG-I (*DDX58*), MDA5 (*IFIH1*), *MAVS*, cGAS (*MB21DB1*), STING (*TMEM173*), *TBK1*, *IRF3*, or *IRF7* for 14 days under puromycin selection (10 μg/ml). All sgRNA targeting sequences were provided in Supplementary Table S1.

Viruses and virus infections

All human and animal RV strains used in this study were propagated in MA104 cells and RV infection was performed as previously described (19). Recombinant VSV (strain Indiana) expressing GFP was a kind gift from Dr. Jack Rose (Yale University) and propagated and titrated in BHK cells. Coxsackievirus B3 strain was propagated and titrated in Hela cells. Lentiviruses used in this study include pLenti-C-Myc-DDK-P2A-ING3, pLenti-C-mGFP-ING3, and lenti-CRISPR_v2 vector encoding Cas9 and sgRNA against *CHD8*, *COG7*, *ING3*, *KDSR*, *MGAT1*, *MMGT1*, *MYC*, *PHIP*, *RALGAPB*, RIG-I (*DDX58*), MDA5 (*IFIH1*), *MAVS*, cGAS (*MB21DB1*), STING (*TMEM173*), *TBK1*, *IRF3* or *IRF7*. All of them were packaged in HEK293T cells by co-transfection with psPAX2 and pMD2.G as previously described (20). Supernatants were collected at 48 and 72 h post transfection, passed through a 450 nm filter, and added to target cells in the presence of polybrene (8 μg/ml).

Protein analysis

Western blot was performed using primary antibodies against cGAS (Cell Signaling Technology (CST), 15102S, 1:1000), EZH2 (CST, 5246S, 1:1000), GAPDH (CST, 5174S, 1:1000), H3K27me3 (CST, 9733S, 1:1000), Histone H3 (CST, 14269S, 1:1000), ING3 (Sigma-Aldrich, HPA067575, 1:500), IRF3 (CST, 11904S, 1:1000), IRF7 (CST, 72073S, 1:1000), MAVS (CST, 3993S, 1:1000), MDA5 (CST, 5321S,1:1000), RIG-I (CST, 3743S, 1:1000), STING (CST, 13647S, 1:1000) and TBK1 (CST, 3504S, 1:1000). IFN-λ secretion was quantified by the DuoSet ELISA for Human IL-29/IL-28B (IFNL-1/3) kit (R&D Systems).

Reverse transcription and quantitative PCR

Total RNA was extracted from cells using RNeasy Mini kit (Qiagen) and reverse transcription was performed using High Capacity RT kit and random hexamers as previously described (21). Quantitative PCR was performed on Stratagene Mx3005P (Agilent) with a 25 μl reaction, composed of 50 ng of cDNA, 12.5 μl of Power SYBR Green master mix (Applied Biosystems), and 200 nM both forward and reverse primers. All SYBR Green primers used in this study (Supplementary Tables S2 and S3) have been validated with both dissociation curves and electrophoresis of the correct amplicon size. Taqman primers used in this study were also provided in Supplementary Table S2.

RNA sequencing

Total RNA from WT and *ING3* KO HT-29 cells was extracted using the RNeasy Mini Kit (Qiagen). RNA sample quality was examined by NanoDrop spectrophotometer (Thermo Fisher) and Bioanalyzer 2100 (Agilent). Total RNA sequencing libraries were constructed and sequenced on BGISEQ-500 platforms. Clean reads were generated by SOAPnuke (v.1.5.6) with the following parameters: -n 0.001 -l 20 -q 0.4 -A 0.25. The SE reads (50 bp) were aligned to the hg38 build using Bowtie2 (v.4.8.2 20140120) to map clean reads to reference gene and using HISAT2 (v.4.8.2) to reference genome (Homo_sapiens GCF_000001405.38_GRCh38.p12) with the following parameters: –phred64 –sensitive -I 1 -X 1000. KEGG (v.93.0) was used for gene annotation. Fragments per kilobase of transcript per million (FKPM) reads were counted using Subread (v.1.4.6), and differential gene expression analysis was performed using DESeq2 (v.1.16.1) based on the non-parametric NOIseq method (22). The FKPM information was provided as Supplementary Dataset 1.

Preparation of dsRNA

Cells from two biological replicates were lysed in TRIzol reagent (Invitrogen) and kept at −80°C until use. Total cellular RNA from wild-type or *ING3* KO HT-29 cells was extracted using Direct-zol RNA Miniprep Kit (Zymo Research). Extracted RNA was treated enzymatically with RNase-free DNase I (Ambion) 37°C for 1 hour, and recovered using RNA Clean & Concentrator-25 (Zymo Research). RNA quantification was done using a Qubit RNA Broad Range Assay kit and Qubit fluorometer according to the manufacturer's instructions. DsRNA was prepared by treating 100 mg of total cellular RNA in 0.3 M NaCl buffer with 200 units of S1 nuclease (Thermo Fisher Scientific) at 37°C for 45 min (23), and size of dsRNA longer than 200 nucleotides was purified and used in the transfection experiments.

Chromatin immunoprecipitation

ChIP was performed following the protocol of Pierce™ Magnetic ChIP Kit (Thermo Fisher Scientific, 26157). Briefly, WT and *ING3* KO HT-29 cells complemented with empty vector or pLenti-C-Myc-DDK-P2A-ING3 were cross-linked with 1% formaldehyde for 10 min at room temperature. The cells were treated using Membrane Extraction Buffer containing protease/phosphatase inhibitors and incubated on ice for 10 min. After centrifuge, cells were resuspended with MNase Digestion Buffer Working Solution and MNase in 37°C for 15 min. The lysate was then sonicated for 10 cycles at 30% amplitude (30 s ON and 30 s OFF). The sonicated samples were then diluted in ChIP dilution buffer and used for the immunoprecipitation with anti-Myc (Thermo Fisher Scientific, MA116637). The EZH2, H3K27me3, and H3K9me3 ChIP was performed using the following antibodies: EZH2 (CST, 5246S), H3K27me3 (CST, 9733S), H3K9me3 (Abcam, ab8898), Histone H3 (CST, 4620S). After an over-night incubation with antibody, ChIP Grade Protein A/G Magnetic Beads were added to each IP and incubate at 4°C overnight with mixing. The bound DNA was washed sequentially with IP Elution Buffer and reverse cross-linked using NaCl for 1.5 hr at 65°C. The eluted DNA was purified and used for qPCR reactions. QPCR was performed as described above using primers described in Supplementary Table S4.

Immunoprecipitation

Immunoprecipitation was performed as described previously (24). Briefly, cells were washed by ice-cold PBS for 3 times, then lysed by NP40 cell lysis buffer (Invitrogen, FNN0021) supplemented with protease inhibitor cocktail (Thermo Scientific, 78430) and PMSF (Santa Cruz, sc-482875) on ice for 30 min. Cell lysates were clarified by centrifugation at 14 000 g for 10 min at 4°C. The lysates were incubated with 2 μg of anti-EZH2 antibody (CST, 5246S), or normal rabbit IgG (Millipore, 12-370) at 4°C overnight. In the meantime, Dynabeads (Invitrogen, 10004D) were incubated with 5% BSA diluted in PBS to reduce the non-specific background at 4°C overnight. Next, the antibody-lysates mixture was added to the dynabeads at 4°C for 4 h. The complex was washed with ice-cold NP40 lysis buffer for three times before the complex was eluted in 2× Laemmli sample buffer (Bio-Rad, 1610737) at 95°C for 5 min.

Statistical analysis

All bar graphs were displayed as means ± SEM. Statistical significance of data in Figures 1D, 2B, E, 4A–D, Supplementary Figures S2F, and S3D was calculated by Student's *t* test using Prism 8 (GraphPad). Statistical significance of data in Figures 1A–C, 2C–D, 3B–D, Supplementary Figures S1E, and S3C was calculated by pairwise ANOVA using Prism 8. All data were presented as asterisks (*$P \leq 0.05$; **$P \leq 0.01$; ***$P \leq 0.001$). All experiments other than Figure 2A and Supplementary Figure S1C have been repeated at least twice. The transcriptome analysis of wild-type and *ING3* KO HT-29 cells in Figure 2A was performed once in duplicate. The raw data is included in Dataset S1.

RESULTS

In a genome-wide CRISPR/Cas9 loss-of-function screen for rotavirus (RV) dependence factors, we identified a number of host genes with novel pro-viral functions (25). Here, we performed a focused validation screen using a lentivirus based pooled CRISPR/Cas9 knockout (KO) approach. Genetic deletion of *ING3* in H1-Hela cells decreased RV gene NSP5 mRNA levels and viral titers as compared to mock transduced cells (Supplementary Figure S1A, B). We next generated single clonal *ING3* KO HT-29 cells, a human colonic epithelial cell line commonly used for RV research (26). RV replication was significantly reduced (>100-fold) in three independent *ING3* KO clones (Figure 1A). These cells did not exhibit noticeable defects in survival or proliferation (data not shown). Complete *ING3* deletion was confirmed by Sanger sequencing of the genomic locus targeted by Cas9 and western blot (Supplementary Figure S1C, D). Compared to the wild-type HT-29 cells, *ING3* KO cells had substantially lower levels (∼500-fold) of bovine RV UK strain replication, as measured by RV RNA levels and virus titers (Figure 1B, C). ING3 supported the replication of a variety of human and animal RV strains (Figure 1D). Importantly, transduction of *ING3* KO HT-29 cells with lentiviruses encoding monomeric GFP (mGFP)-tagged ING3 partially restored RV replication (Figure 1B, C and Supplementary Figure S1D). Functional complementation of genetic deletion of *ING3* was also verified by a lentiviral vector that encodes Myc-tagged ING3 (Supplementary Figure S1E).

In addition to RV, which is a double-stranded (ds) RNA virus, *ING3* KO cells were also highly resistant to infections by single-stranded (ss)RNA (+) and ssRNA (-) viruses such as coxsackievirus B3 strain and vesicular stomatitis virus, respectively (Supplementary Figure S2A), suggesting that ING3 may regulate a cellular pathway common to different RNA virus families. To shed light on the molecular mechanisms of the broad pro-viral effect of ING3, we profiled the cellular transcriptomes of wild-type and two independent clones of *ING3* KO HT-29 cells by RNA-sequencing. Both gene ontology and KEGG pathway analysis revealed up-regulation of pathways mediating innate immune activation towards viruses and endogenous stimuli in *ING3* KO cells (Supplementary Figure S2B-C). The

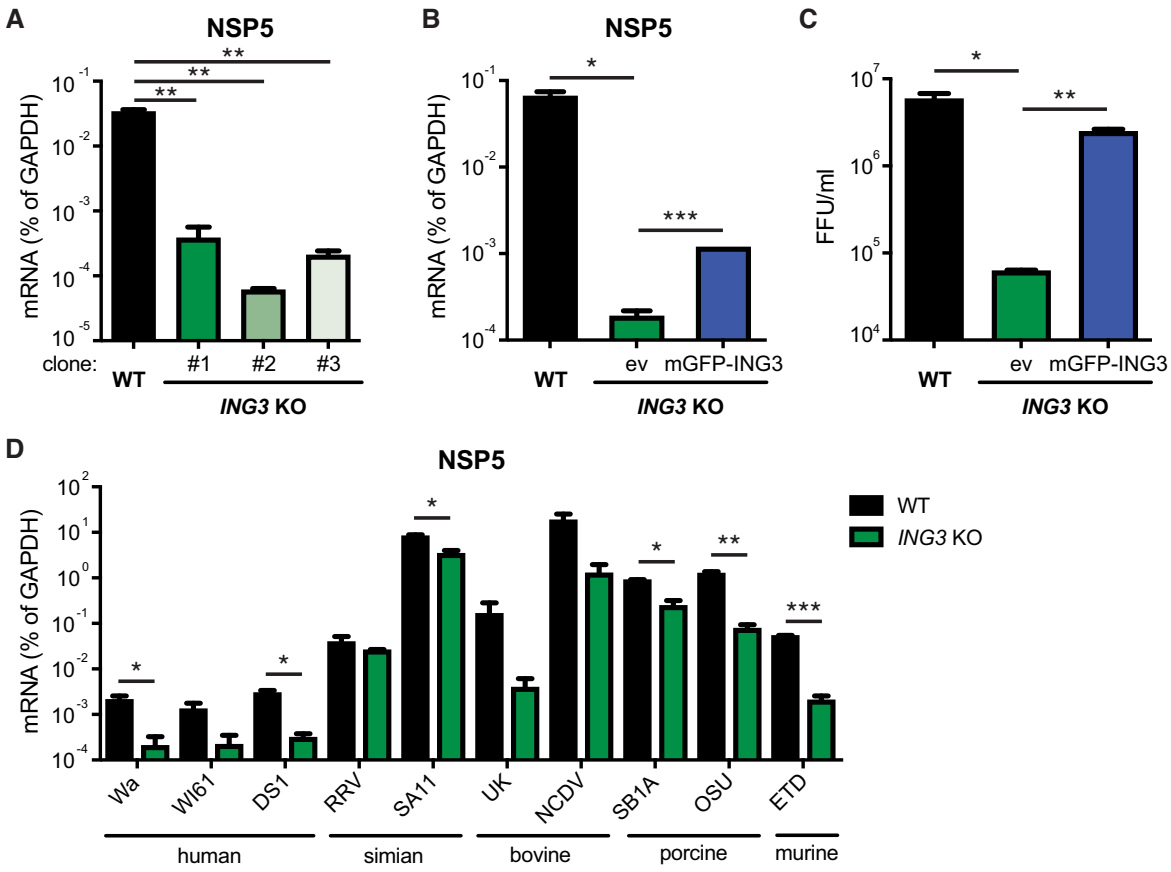

Figure 1. *ING3* deficient cells are resistant to RV infection. (**A**) WT and *ING3* KO (clones #1, #2, and #3) HT-29 cells were infected with bovine RV UK strain (MOI = 1) for 24 h. RV *NSP5* level was measured by RT-qPCR and normalized to that of *GAPDH*. (**B**) WT and *ING3* KO HT-29 cells transduced with lentiviruses either in empty vector (ev) or encoding mGFP-ING3 were infected with bovine RV UK strain (MOI = 1) for 24 h. RV *NSP5* level was measured by RT-qPCR and normalized to that of *GAPDH*. (**C**) Same as (B) except that at 24 h post infection, infectious RV titers were determined by a focus-forming unit assay. (**D**) WT and *ING3* KO HT-29 cells were infected with a panel of different human and animal RV strains (MOI = 1) for 24 h. RV *NSP5* level was measured by RT-qPCR and normalized to that of *GAPDH*. For all panels, experiments were repeated at least three times with similar results. Data are represented as mean ± SEM. Statistical significance is from pooled data of the multiple independent experiments (*$P \leq 0.05$; **$P \leq 0.01$; ***$P \leq 0.001$).

expression of canonical interferon (IFN)-stimulated genes (ISGs) such as *IFI44L* and *IFITM1*, was up-regulated by over 100-fold in *ING3* KO cells compared to wild-type HT-29 cells (Figure 2A). This ISG signature was confirmed by reverse transcriptase-quantitative polymerase chain reaction (RT-qPCR) (Figure 2B and Supplementary Figure S2D). Consistent with our previous observation with primary intestinal epithelial cells and cell lines (19), type III IFN expression was preferentially induced in *ING3* KO cells compared to wild-type HT-29 cells (Figure 2C and Supplementary Figure S2E). In the absence of virus infection, we detected robust IFN-λ secretion in the supernatants of *ING3* KO HT-29 cells by enzyme-linked immunosorbent assay (ELISA) (Figure 2D). IFN-λ mRNA and secreted cytokine levels were partially restored to homeostatic status upon re-expression of mGFP-tagged or Myc-tagged ING3 (Figure 2C, D).

We reasoned that the heightened IFN and ISG responses could mediate broad resistance to virus infections in *ING3* KO cells. Indeed, treatment of cells with a JAK kinase inhibitor ruxolitinib, which effectively blocks STAT1 phosphorylation (27), led to a dramatic reduction in IFN and MX1 expression (Supplementary Figure S2F) and partially restored the susceptibility to RV infection in *ING3* KO HT-29 cells (Figure 2E). Taken together, these data establish ING3 as a previously unknown regulator of IFN signaling.

We next dissected the cellular pathway required for IFN induction triggered by *ING3* deficiency. Since ING3 mediates the repair of double-strand DNA breaks (18), our data are reminiscent of findings with *STAG2* (25) and *Banf1* (28), of which genetic ablation leads to STING activation and IFN induction. Hence we posited that the cytoplasmic DNA sensing pathway might be involved in ING3's innate immune regulatory activity. We used CRISPR/Cas9 editing to knock out major components in the IFN induction signaling pathway, including RIG-I, MDA5, MAVS, cGAS, STING, TBK1, IRF3 and IRF7. The levels of these proteins were efficiently depleted in *ING3* KO cells (Figure 3A). Surprisingly, deletion of the dsRNA sensor MDA5 or downstream factors of MDA5, including MAVS, TBK1, and IRF3, led to a restoration of the baseline IFN mRNA levels (Figure 3B). Consistently, CRISPR-mediated inhibi-

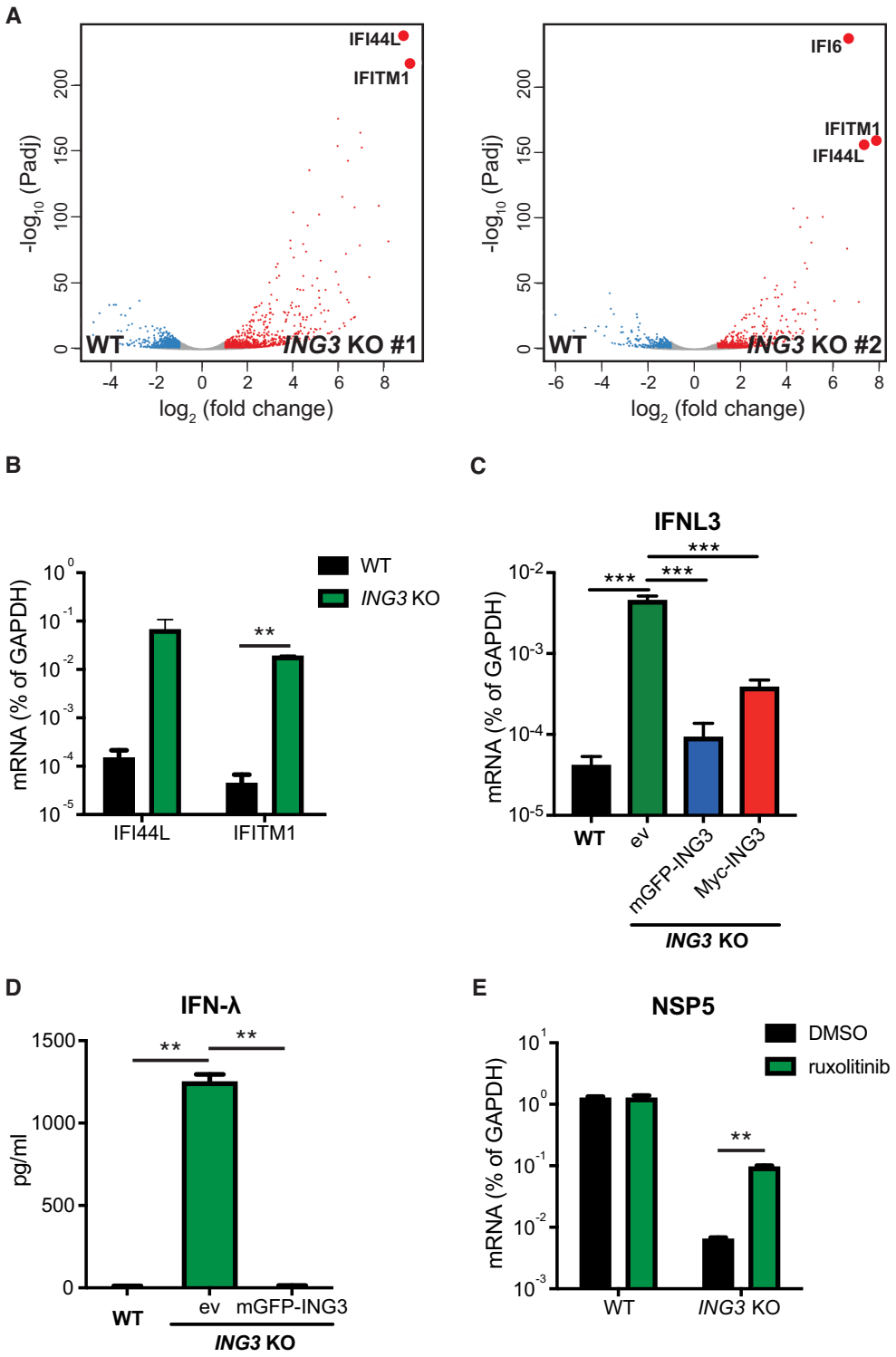

Figure 2. Loss of *ING3* induces robust IFN and ISG expression. (**A**) Volcano plots of RNA-sequencing analysis of WT and *ING3* KO (clones #1 and #2) HT-29 cells. Genes that were up-regulated in *ING3* KO cells are highlighted in red, and the highly induced ISGs were marked with more prominent red dots (Padj: adjusted p-value). (**B**) *IFI44L* and *IFITM1* transcript levels were measured by RT-qPCR and normalized to that of *GAPDH* in WT and *ING3* KO HT-29 cells. (**C**) *IFNL3* transcript level was measured by RT-qPCR and normalized to that of *GAPDH* in WT and *ING3* KO HT-29 cells transduced with lentiviruses in empty vector (ev), encoding mGFP-ING3, or encoding Myc-ING3. (**D**) Same as (C) except that cell culture supernatants were collected and secreted IFN-λ levels were measured by ELISA. (**E**) WT and *ING3* KO HT-29 cells were treated with vehicle control DMSO or JAK inhibitor ruxolitinib (100 nM) for 24 hr and infected with RV (MOI = 1) for another 24 h. RV *NSP5* level was measured by RT-qPCR and normalized to that of *GAPDH*. For all panels except A, experiments were repeated at least three times with similar results. Figure A was performed once with technical duplicates. Raw data is listed in Dataset S1. Data are represented as mean ± SEM. Statistical significance is from pooled data of the multiple independent experiments (**$P \leq 0.01$; ***$P \leq 0.001$).

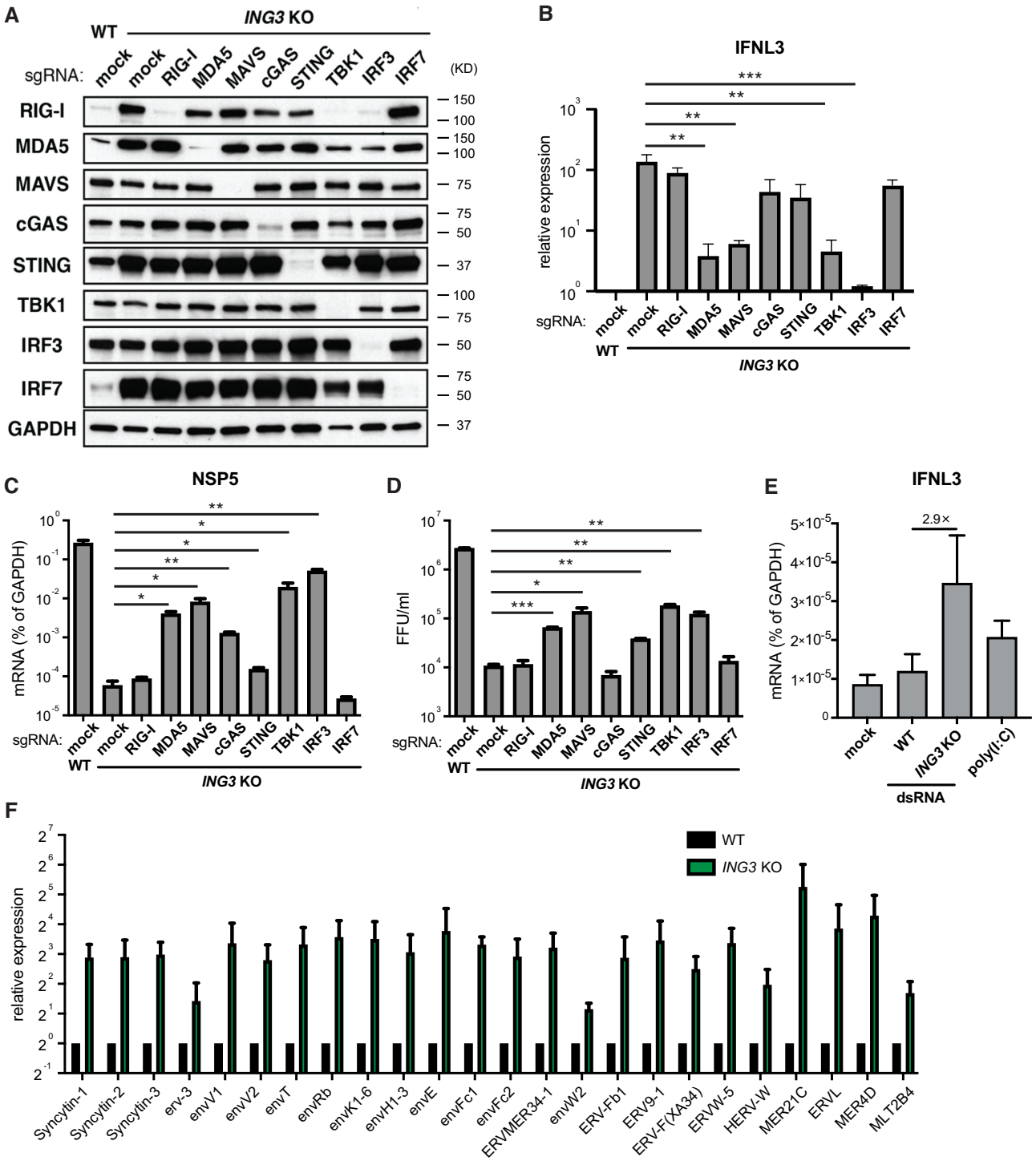

Figure 3. ERVs activate MDA5-MAVS signaling in *ING3* KO cells. (**A**) WT and *ING3* KO HT-29 cells were transduced with lentiviruses encoding Cas9 and single-guide RNAs (sgRNAs) against the indicated genes and selected under puromycin for 10 days. Cell lysates were harvested and the indicated proteins levels were examined by western blot. (**B**) Same as (A) except that the cellular RNA was harvested and *IFNL3* level was measured by RT-qPCR and normalized to that of *GAPDH*. (**C**) Same as (A) except that cells were infected with RV (MOI = 1) for 24 hr. RV *NSP5* level was measured by RT-qPCR and normalized to that of *GAPDH*. (**D**) Same as (C) except that at 24 hr post infection, infectious RV titers were determined by a focus-forming unit assay. (**E**) WT HT-29 cells were transfected with LyoVec in complex with dsRNA longer than 200 nucleotides from WT HT-29 cells (10 ng), dsRNA from *ING3* KO HT-29 cells (10 ng), or high-molecular weight poly(I:C) (100 ng) for 24 hr. *IFNL3* transcript level was measured by RT-qPCR and normalized to that of *GAPDH*. (**F**) Indicated ERV transcript levels were measured by RT-qPCR and normalized to that of *GAPDH* in WT and *ING3* KO HT-29 cells. For all panels, experiments were repeated at least three times with similar results. Data are represented as mean ± SEM. Statistical significance is from pooled data of the multiple independent experiments (*$P \leq 0.05$; **$P \leq 0.01$; ***$P \leq 0.001$).

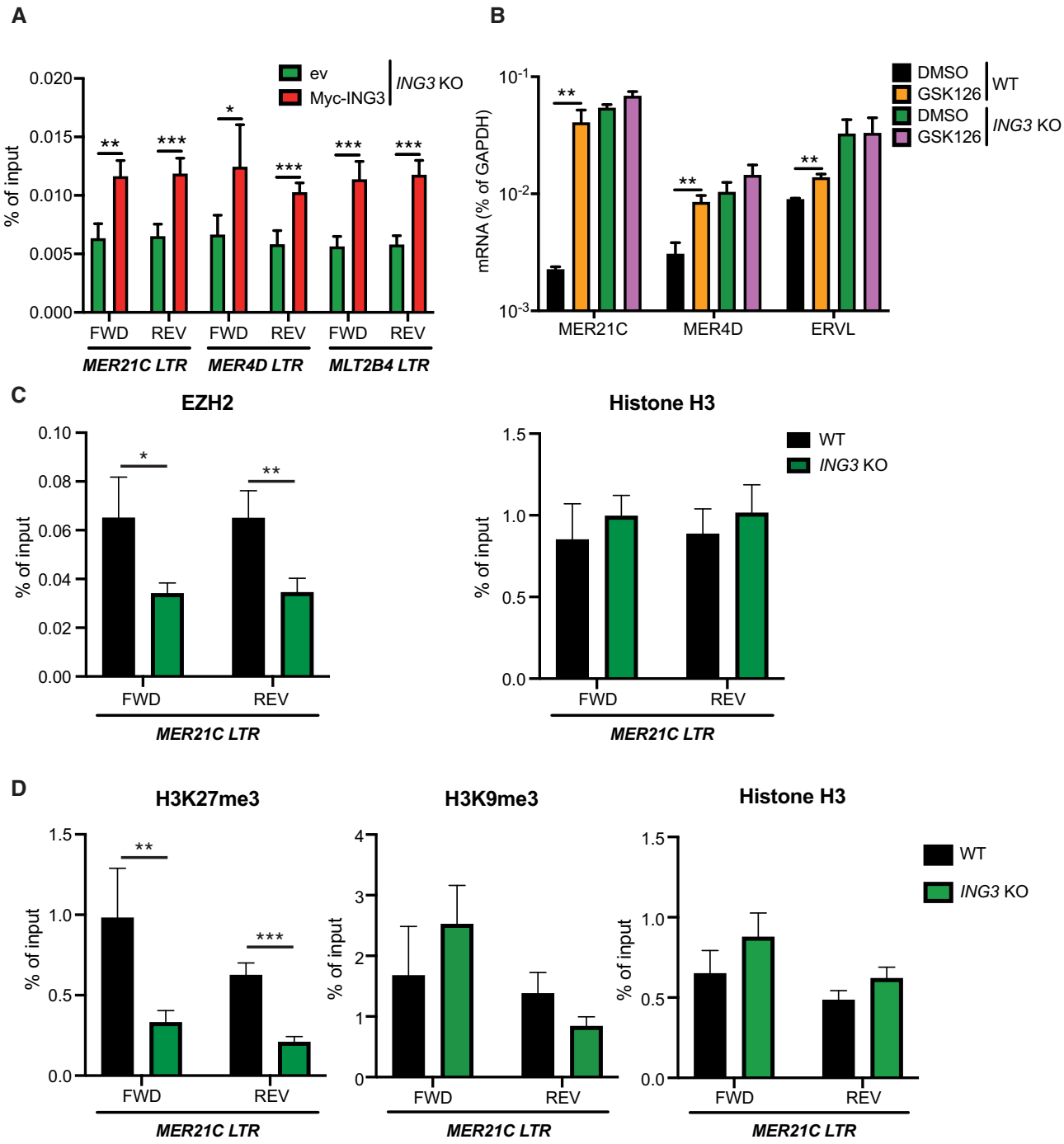

Figure 4. ING3 recruits EZH2 and H3K27 trimethylation to the ERV promoters. (**A**) *ING3* KO HT-29 cells transduced with lentiviruses either in empty vector (ev) or encoding Myc-ING3 were subjected to chromatin immunoprecipitation (ChIP) using an anti-Myc antibody and RT-qPCR assay to examine the forward (FWD) and reverse (REV) LTR regions of indicated ERVs. (**B**) WT and *ING3* KO HT-29 cells were cultured with vehicle control DMSO or EZH2 inhibitor GSK126 (10 μM) for 6 days. *MER21C*, *MER4D* and *ERVL* transcript levels were measured by RT-qPCR and normalized to that of *GAPDH*. (**C**) WT and *ING3* KO HT-29 cells were subjected to ChIP using anti-EZH2 or Histone H3 antibodies and RT-qPCR assay to examine the forward (FWD) and reverse (REV) LTR regions of *MER21C*. (**D**) Same as (C) except that H3K27 trimethylation (H3K27me3) or H3K9 trimethylation (H3K9me3) antibodies were used in ChIP instead of EZH2. For all panels, experiments were repeated at least three times with similar results. Data are represented as mean ± SEM. Statistical significance is from pooled data of the multiple independent experiments (*$P \leq 0.05$; **$P \leq 0.01$; ***$P \leq 0.001$).

tion of the MDA5-MAVS-TBK1-IRF3 signaling enhanced intracellular RV RNA levels and virus titers in the *ING3* KO cells (Figure 3C, D). In contrast, knocking out cytosolic DNA sensor cGAS or its adaptor protein STING had a relatively modest effect on IFN expression and virus infection (Figure 3B–D).

To further probe the role of dsRNAs in IFN responses in WT and *ING3* KO cells, we used S1 nuclease to generate dsRNAs from total cellular RNAs (23). When transfected into cells, dsRNA from *ING3* KO HT-29 cells induced higher (2.9-fold) IFN mRNA levels than dsRNA of wild-type HT-29 cells (Figure 3E). We next sought to determine the nature of cellular dsRNA ligands that activate MDA5 signaling in *ING3* KO cells. A number of potential sources for dsRNAs are known, including circular RNA, mitochondrial RNA, and retrotransposon elements such as ALU and ERVs (29–31). To assess whether any known TEs were regulated upon *ING3* depletion, we quantified the levels of 24 individual ERVs through RT-qPCR, spanning human ERV classes I and III (32). Most ERVs examined were up-regulated by 8–16-fold in *ING3* KO cells compared to wild-type HT-29 cells (Figure 3F). Augmented expression of multiple ERVs was verified in a separate *ING3* KO clone (Supplementary Figure S3A). In contrast, transcripts from other TEs such as ALU and LINE-1 were not affected (Supplementary Figure S3B), and complementation of *ING3* KO cells with exogenously introduced ING3 restored the expression of ERVs to homeostatic levels (Supplementary Figure S3C), highlighting the specific ING3 targeting of ERVs. To exclude the possible secondary effect of IFN induction on ERV transcription, we measured the mRNA levels of *ERVs*, which were not induced by IFN-β treatment as canonical ISGs OAS3 and MX1 (Supplementary Figure S3D).

Next, we tested whether ING3 is present at the ERV promoters by chromatin immunoprecipitation (ChIP). With a weak antibody to detect endogenous ING3 (Supplementary Figure S1D), we turned to the *ING3* KO cells complemented with Myc-tagged ING3 (Supplementary Figure S1E). Anti-Myc ChIP in rescued cells revealed enriched occupancy of ING3 at the LTR regions of several ERVs, including *MER21C*, *MER4D* and *MLT2B4* (Figure 4A), all of which were up-regulated upon *ING3* deletion (Figure 3F). In contrast, anti-Myc ChIP assay in rescued cells showed that ING3 did not bind to the promotor regions of LINE-1 and ALU elements (Supplementary Figure S4A), both of which were not activated in *ING3* KO HT-29 cells (Figure 3F). In addition, anti-Myc ChIP assay also specifically detected ING3 binding at the *RPSA* promoter as previously described (33), and this was highly specific to Myc-ING3 expressing cells and not the control *ING3* KO cells (Supplementary Figure S4B). ING3 was reported to interact with multiple epigenetic regulators, including KAT5/TIP60 complex, DNA methyltransferase 1 associated protein 1, and polycomb-group proteins (17,34). To define the mechanism of how ING3 potentially precludes ERV activation at steady state, we utilized a set of small-molecule inhibitors that target respective histone methyltransferases and demethylases. Treatment of wild-type HT-29 cells with GSK126, a highly selective inhibitor of enhancer of zeste homolog 2 (EZH2), an H3K27 methyltransferase (35), resulted in an appreciable increase of MER21C, MER4D, and ERVL expression (Figure 4B), without inducing a global decrease of H3K27 trimethylation (Supplementary Figure S5A). GSK126 treatment did not alter the expression levels of LINE-1 or ALU elements (Supplementary Figure S5B). MER21C expression was not reactivated by histone demethylase inhibitors JIB-04 and GSK-J4 (Supplementary Figure S5C). The enhancing effect of GSK126 treatment on ERV levels was limited in *ING3* KO cells (Figure 4B). Using *ING3* KO HT-29 cells complemented with Myc-ING3, we found that EZH2 coprecipitated with ING3 (Supplementary Figure S5D). We then detected by ChIP-qPCR that the degree of EZH2 binding reduced in *ING3* KO HT-29 cells compared to wild-type cells (Figure 4C). These data suggest that ING3 likely recruits EZH2 to the ERV sites for transcriptional suppression.

Consistent with EZH2 binding, we measured hallmarks of chromatin repression and found more H3K27 trimethylation but not H3K9 trimethylation at the *MER21C* promoter in wild-type HT-29 cells and it was diminished significantly in the absence of *ING3* (Figure 4D). Although DNA methyltransferase inhibitor treatment was previously shown to induce ERV activation and IFN production (36,37), the methylation status of the *MER21C* promoter was not altered in the presence or absence of *ING3* (data not shown). Further, treatment of wild-type cells with 5-aza-2′-deoxycytidine, a DNA methyltransferase inhibitor, did not trigger ERV reactivation (data not shown), suggesting a different mechanism of ING3-mediated epigenetic silencing. In summary, our data demonstrate that ING3 is a new 'molecular checkpoint' of a broad range of ERVs, whose expression needs to be tightly regulated to prevent autonomous innate immune activation.

DISCUSSION

Here, using a genome-wide CRISPR/Cas9 screen, RNA sequencing, and ChIP, we determined that ING3 functions as a novel 'gatekeeper' of ERV expression and IFN homeostasis. *ING3* deficiency leads to ERV de-suppression, activation of the MDA5-MAVS signaling, and excessive IFN production. Of note, both ING1 and ING5, members in the same family as ING3, were also among the top 200 hits of our CRISPR/Cas9 screen (25). Whether they play a similar or distinct role in ERV suppression remains to be determined.

Although TIP60 is known to associate with ING3 to regulate gene expression (17,34), *TIP60* deficiency led to a loss of H3K9 trimethylation and activation of the ERV promoters (14). However, we found that in the case of ING3, H3K27 trimethylation via EZH2 but not H3K9 trimethylation is the predominant repressive marker (Figure 4B-D), suggesting a distinct silencing mechanism. Since ING3 encodes a highly conserved PHD domain (38), we speculate that unlike the other epigenetic regulators, ING3 is able to directly recognize and bind DNA sequences and motives. In future studies, it will be of interest to determine whether there are significant overlaps in the ERVs targeted by KAP1, TIP60, KDM5B, FBXO44, versus ING3.

The potential limitations of the study include the specificity of ING3 targeting ERVs and whether the IFN induc-

tion is directly mediated through ERVs. Specifically, not all repetitive elements seem to be regulated by ING3, the underlying mechanisms of which we will examine by ChIP-seq analysis in future studies. Also, we have not definitively shown that the dsRNA ligands directly originated from ERV sequences. To address this problem, we may be able to take advantage of S1 nuclease digestion to enrich cytoplasmic dsRNA molecules and couple with RNA-seq analysis.

In the human population, the occurrence of *ING3* loss-of-function mutations is substantially under-represented (observed-expected ratio of loss-of-function variants in *ING3* = 0.07; missense variants = 0.56) according to the Genome Aggregation Database (39). This suggests a highly detrimental outcome of pre-mature stop codons in *ING3*, especially because loss of Ing3 has been associated with embryonic lethality in mice (40). These alleles are potentially too rare to be directly linked to autoimmune diseases via genome-wide association studies, but our results and the regulatory mechanism described can influence MDA5 activation thresholds in humans and hence might affect the likelihood of some autoimmune disorders or cancer progression. Further *in vivo* studies will test whether selective inhibition of ING3 induces viral mimicry in cancer cells and promotes anti-tumor immunity.

DATA AVAILABILITY

Raw data is deposited and available at GEO (GSE166219).

SUPPLEMENTARY DATA

Supplementary Data are available at NAR Online.

ACKNOWLEDGEMENTS

The authors would like to thank Dr. Qin Yan (Yale University) and Drs. Michael Diamond, Jacco Boon, and Sebla Kutluay (Washington University in St. Louis) for constructive comments and suggestions.

FUNDING

National Institutes of Health (NIH) [DDRCC grant P30 DK052574, NIH grants R00 AI135031 and R01 AI150796 to S.D., NIH grant R01 AI125249 and VA Merit grant GRH0022 to H.B.G., NIH grant R01 AI141970]; Burroughs Wellcome Fund Investigators in the Pathogenesis of Infectious Disease (to J.E.C.) NIH [R01 AI029646 and AI130222 to S.M.B.]. Funding for open access charge: National Institutes of Health (NIH) [DDRCC grant P30 DK052574, NIH grants R00 AI135031 and R01 AI150796 to S.D., NIH grant R01 AI125249 and VA Merit grant GRH0022 to H.B.G., NIH grant R01 AI141970]; Burroughs Wellcome Fund Investigators in the Pathogenesis of Infectious Disease (to J.E.C.) NIH [R01 AI029646 and AI130222 to S.M.B.].
Conflict of interest statement. None declared.

REFERENCES

1. de Koning,A.P., Gu,W., Castoe,T.A., Batzer,M.A. and Pollock,D.D. (2011) Repetitive elements may comprise over two-thirds of the human genome. *PLoS Genet.*, **7**, e1002384.
2. Lander,E.S., Linton,L.M., Birren,B., Nusbaum,C., Zody,M.C., Baldwin,J., Devon,K., Dewar,K., Doyle,M., FitzHugh,W. *et al.* (2001) Initial sequencing and analysis of the human genome. *Nature*, **409**, 860–921.
3. Wicker,T., Sabot,F., Hua-Van,A., Bennetzen,J.L., Capy,P., Chalhoub,B., Flavell,A., Leroy,P., Morgante,M., Panaud,O. *et al.* (2007) A unified classification system for eukaryotic transposable elements. *Nat. Rev. Genet.*, **8**, 973–982.
4. Kassiotis,G. (2014) Endogenous retroviruses and the development of cancer. *J. Immunol.*, **192**, 1343–1349.
5. Kury,P., Nath,A., Creange,A., Dolei,A., Marche,P., Gold,J., Giovannoni,G., Hartung,H.P. and Perron,H. (2018) Human endogenous retroviruses in neurological diseases. *Trends Mol. Med.*, **24**, 379–394.
6. Grow,E.J., Flynn,R.A., Chavez,S.L., Bayless,N.L., Wossidlo,M., Wesche,D.J., Martin,L., Ware,C.B., Blish,C.A., Chang,H.Y. *et al.* (2015) Intrinsic retroviral reactivation in human preimplantation embryos and pluripotent cells. *Nature*, **522**, 221–225.
7. Howard,G., Eiges,R., Gaudet,F., Jaenisch,R. and Eden,A. (2008) Activation and transposition of endogenous retroviral elements in hypomethylation induced tumors in mice. *Oncogene*, **27**, 404–408.
8. Wolf,D. and Goff,S.P. (2009) Embryonic stem cells use ZFP809 to silence retroviral DNAs. *Nature*, **458**, 1201–1204.
9. Ecco,G., Cassano,M., Kauzlaric,A., Duc,J., Coluccio,A., Offner,S., Imbeault,M., Rowe,H.M., Turelli,P. and Trono,D. (2016) Transposable elements and their KRAB-ZFP controllers regulate gene expression in adult tissues. *Dev. Cell*, **36**, 611–623.
10. Liu,S., Brind'Amour,J., Karimi,M.M., Shirane,K., Bogutz,A., Lefebvre,L., Sasaki,H., Shinkai,Y. and Lorincz,M.C. (2014) Setdb1 is required for germline development and silencing of H3K9me3-marked endogenous retroviruses in primordial germ cells. *Genes Dev.*, **28**, 2041–2055.
11. Rowe,H.M., Jakobsson,J., Mesnard,D., Rougemont,J., Reynard,S., Aktas,T., Maillard,P.V., Layard-Liesching,H., Verp,S., Marquis,J. *et al.* (2010) KAP1 controls endogenous retroviruses in embryonic stem cells. *Nature*, **463**, 237–240.
12. Sadic,D., Schmidt,K., Groh,S., Kondofersky,I., Ellwart,J., Fuchs,C., Theis,F.J. and Schotta,G. (2015) Atrx promotes heterochromatin formation at retrotransposons. *EMBO Rep.*, **16**, 836–850.
13. Treger,R.S., Pope,S.D., Kong,Y., Tokuyama,M., Taura,M. and Iwasaki,A. (2019) The lupus susceptibility locus Sgp3 encodes the suppressor of endogenous retrovirus expression SNERV. *Immunity*, **50**, 334–347.
14. Rajagopalan,D., Tirado-Magallanes,R., Bhatia,S.S., Teo,W.S., Sian,S., Hora,S., Lee,K.K., Zhang,Y., Jadhav,S.P., Wu,Y. *et al.* (2018) TIP60 represses activation of endogenous retroviral elements. *Nucleic Acids Res.*, **46**, 9456–9470.
15. Zhang,S., Cai,W., Liu,X., Thakral,D., Luo,J., Chan,L., McGeary,M., Song,E., Blenman,K., Micevic,G. *et al.* (2021) KDM5B promotes immune evasion by recruiting SETDB1 to silence retroelements. *Nature*, **598**, 682–687.
16. Shen,J.Z., Qiu,Z., Wu,Q., Finlay,D., Garcia,G., Sun,D., Rantala,J., Barshop,W., Hope,J.L., Gimple,R.C. *et al.* (2020) FBXO44 promotes DNA replication-coupled repetitive element silencing in cancer cells. *Cell*, **184**, 352–369.
17. Doyon,Y., Cayrou,C., Ullah,M., Landry,A.J., Cote,V., Selleck,W., Lane,W.S., Tan,S., Yang,X.J. and Cote,J. (2006) ING tumor suppressor proteins are critical regulators of chromatin acetylation required for genome expression and perpetuation. *Mol. Cell*, **21**, 51–64.
18. Mouche,A., Archambeau,J., Ricordel,C., Chaillot,L., Bigot,N., Guillaudeux,T., Grenon,M. and Pedeux,R. (2019) ING3 is required for ATM signaling and DNA repair in response to DNA double strand breaks. *Cell Death Differ.*, **26**, 2344–2357.
19. Ding,S., Zhu,S., Ren,L., Feng,N., Song,Y., Ge,X., Li,B., Flavell,R.A. and Greenberg,H.B. (2018) Rotavirus VP3 targets MAVS for degradation to inhibit type III interferon expression in intestinal epithelial cells. *eLife*, **7**, e39494.
20. Ding,S., Khoury-Hanold,W., Iwasaki,A. and Robek,M.D. (2014) Epigenetic reprogramming of the type III interferon response potentiates antiviral activity and suppresses tumor growth. *PLoS Biol.*, **12**, e1001758.
21. Li,B., Ding,S., Feng,N., Mooney,N., Ooi,Y.S., Ren,L., Diep,J., Kelly,M.R., Yasukawa,L.L., Patton,J.T. *et al.* (2017) Drebrin restricts

rotavirus entry by inhibiting dynamin-mediated endocytosis. *PNAS*, **114**, E3642–E3651.
22. Love,M.I., Huber,W. and Anders,S. (2014) Moderated estimation of fold change and dispersion for RNA-seq data with DESeq2. *Genome Biol*, **15**, 550.
23. Beiting,D.P., Peixoto,L., Akopyants,N.S., Beverley,S.M., Wherry,E.J., Christian,D.A., Hunter,C.A., Brodsky,I.E. and Roos,D.S. (2014) Differential induction of TLR3-dependent innate immune signaling by closely related parasite species. *PLoS One*, **9**, e88398.
24. Ding,S., Mooney,N., Li,B., Kelly,M.R., Feng,N., Loktev,A.V., Sen,A., Patton,J.T., Jackson,P.K. and Greenberg,H.B. (2016) Comparative proteomics reveals strain-specific β-TrCP degradation via rotavirus NSP1 hijacking a host cullin-3-Rbx1 complex. *PLoS Pathog.*, **12**, e1005929.
25. Ding,S., Diep,J., Feng,N., Ren,L., Li,B., Ooi,Y.S., Wang,X., Brulois,K.F., Yasukawa,L.L., Li,X. *et al.* (2018) STAG2 deficiency induces interferon responses via cGAS-STING pathway and restricts virus infection. *Nat. Commun.*, **9**, 1485.
26. Superti,F., Tinari,A., Baldassarri,L. and Donelli,G. (1991) HT-29 cells: a new substrate for rotavirus growth. *Arch. Virol*, **116**, 159–173.
27. Mesa,R.A., Yasothan,U. and Kirkpatrick,P. (2012) Ruxolitinib. *Nat. Rev. Drug Discov.*, **11**, 103–104.
28. Ma,H., Qian,W., Bambouskova,M., Collins,P.L., Porter,S.I., Byrum,A.K., Zhang,R., Artyomov,M., Oltz,E.M., Mosammaparast,N. *et al.* (2020) Barrier-to-autointegration factor 1 protects against a basal cGAS-STING response. *mBio*, **11**, e00136-20.
29. Chen,Y.G., Kim,M.V., Chen,X., Batista,P.J., Aoyama,S., Wilusz,J.E., Iwasaki,A. and Chang,H.Y. (2017) Sensing self and foreign circular RNAs by intron identity. *Mol. Cell*, **67**, 228–238.
30. Chung,H., Calis,J.J.A., Wu,X., Sun,T., Yu,Y., Sarbanes,S.L., Dao Thi,V.L., Shilvock,A.R., Hoffmann,H.H., Rosenberg,B.R. *et al.* (2018) Human ADAR1 prevents endogenous RNA from triggering translational shutdown. *Cell*, **172**, 811–824.
31. Dhir,A., Dhir,S., Borowski,L.S., Jimenez,L., Teitell,M., Rotig,A., Crow,Y.J., Rice,G.I., Duffy,D., Tamby,C. *et al.* (2018) Mitochondrial double-stranded RNA triggers antiviral signalling in humans. *Nature*, **560**, 238–242.
32. Thompson,P.J., Macfarlan,T.S. and Lorincz,M.C. (2016) Long terminal repeats: from parasitic elements to building blocks of the transcriptional regulatory repertoire. *Mol. Cell*, **62**, 766–776.
33. Jacquet,K., Fradet-Turcotte,A., Avvakumov,N., Lambert,J.P., Roques,C., Pandita,R.K., Paquet,E., Herst,P., Gingras,A.C., Pandita,T.K. *et al.* (2016) The TIP60 complex regulates bivalent chromatin recognition by 53BP1 through direct H4K20me binding and H2AK15 acetylation. *Mol Cell*, **62**, 409–421.
34. Doyon,Y., Selleck,W., Lane,W.S., Tan,S. and Cote,J. (2004) Structural and functional conservation of the NuA4 histone acetyltransferase complex from yeast to humans. *Mol. Cell. Biol.*, **24**, 1884–1896.
35. McCabe,M.T., Ott,H.M., Ganji,G., Korenchuk,S., Thompson,C., Van Aller,G.S., Liu,Y., Graves,A.P., Della Pietra,A. 3rd, Diaz,E *et al.* (2012) EZH2 inhibition as a therapeutic strategy for lymphoma with EZH2-activating mutations. *Nature*, **492**, 108–112.
36. Chiappinelli,K.B., Strissel,P.L., Desrichard,A., Li,H., Henke,C., Akman,B., Hein,A., Rote,N.S., Cope,L.M., Snyder,A. *et al.* (2015) Inhibiting DNA methylation causes an interferon response in cancer via dsRNA including endogenous retroviruses. *Cell*, **162**, 974–986.
37. Roulois,D., Loo Yau,H., Singhania,R., Wang,Y., Danesh,A., Shen,S.Y., Han,H., Liang,G., Jones,P.A., Pugh,T.J. *et al.* (2015) DNA-demethylating agents target colorectal cancer cells by inducing viral mimicry by endogenous transcripts. *Cell*, **162**, 961–973.
38. Luo,J., Shah,S., Riabowol,K. and Mains,P.E. (2009) The *Caenorhabditis elegans* ing-3 gene regulates ionizing radiation-induced germ-cell apoptosis in a p53-associated pathway. *Genetics*, **181**, 473–482.
39. Lek,M., Karczewski,K.J., Minikel,E.V., Samocha,K.E., Banks,E., Fennell,T., O'Donnell-Luria,A.H., Ware,J.S., Hill,A.J., Cummings,B.B. *et al.* (2016) Analysis of protein-coding genetic variation in 60,706 humans. *Nature*, **536**, 285–291.
40. Fink,D., Yau,T., Nabbi,A., Wagner,B., Wagner,C., Hu,S.M., Lang,V., Handschuh,S., Riabowol,K. and Rulicke,T. (2019) Loss of Ing3 expression results in growth retardation and embryonic death. *Cancers (Basel)*, **12**. 80.